Paraxial Space-Domain Formulation for Surface Fields on a Large Dielectric Coated Circular Cylinder

V. B. Ertürk and R. G. Rojas

***Abstract*—A new method to evaluate the surface fields excited within the paraxial (nearly axial) region of an electrically large dielectric coated circular cylinder is presented. This representation is obtained by performing the Watson's transformation in the standard eigenfunction solution and using the fact that the circumferentially propagating series representation of the appropriate Green's function is periodic in one of its two variables. Therefore, it can be approximated by a Fourier series where the two leading terms of the expansion yield engineering accuracy in most cases. This work can be used in conjunction with a method of moments solution for the design/analysis of conformal microstrip antennas and arrays. Numerical results are presented and compared with a standard eigenfunction expansion.**

***Index Terms*—Coated cylinders, Green's function, paraxial representation.**

I. Introduction

THE STUDY of surface fields, created by a current distribution on the surface of a thin dielectric layer deposited on a perfect electrically conducting (PEC) circular cylinder, serves as a canonical problem for the analysis of conformal microstrip antennas/arrays mounted on dielectric coated arbitrarily convex bodies. A derivation of the rigorous dyadic Green's function using a spectral domain Green's function (radially propagating) for an electric dipole located on the surface of a dielectric coated PEC circular cylinder has been presented by several authors [1]–[5]. This representation is known to have convergence problems for large cylinders and separations between source and observation points. A few asymptotic representations for the dyadic Green's function has been presented to overcome this difficulty [6]–[9].

The uniform theory of diffraction (UTD)-based Green's functions for the surface fields on a dielectric coated circular cylinder derived by Munk [6] were implemented in [7] and [8] and numerical calculations showed that reasonable results can be obtained for large separations if only the leading terms are included. Recently, a steepest descent path (SDP) representation of the dyadic Green's function for the dielectric coated circular cylinder has been presented [9], which is based on a circumferentially (ϕ)-propagating series representation of the appropriate Green's function and its efficient numerical evaluation along a SDP on which the integrand decays most rapidly. This method reduces to the saddle point integration considered in [6]–[8] and in contrast to most asymptotic solutions, the results are valid for arbitrarily small separations of source and field points. However, none of these asymptotic solutions ([6]–[9]) yields accurate results within the paraxial (nearly axial) region. This is a well-known problem that has been observed for PEC and impedance cylinders in the past [10]–[14]. Among these solutions, Boersma and Lee [13] used a two-term Debye approximation for the logarithmic derivatives of Hankel functions and obtained a closed-form solution for a PEC cylinder which remains accurate in the paraxial region. Unfortunately, to the best of our knowledge, it is not possible to obtain such closed-form solutions for a dielectric coated cylinder.

In this paper, a new space-domain representation for the surface fields excited by an elementary current source is presented. These new expressions are valid within the paraxial region as opposed to the previously presented asymptotic solutions [6]–[9]. The essence of this formulation is based on the fact that the ϕ-propagating series representation of the Green's function is periodic in one of its variables after an appropriate change of variables. Hence, it can be approximated by a Fourier series (FS) where the coefficients of this series expansion can be easily obtained by a simple numerical integration algorithm. Based on numerical experimentation, it appears that only the two leading terms of the expansion are necessary in most cases. As expected, the accuracy of the Green's function, as well as the ease of its evaluation, are determined by the type of algorithm used to calculate the FS coefficients. In Section II, the development of this novel approximate Green's function representation, as well as new expressions for the surface fields valid within the paraxial region, are presented. Numerical calculations are presented in Section III, which indicate that the results shown here are valid for arbitrarily small and large separations of source and field points. An $e^{j\omega t}$ time dependence is assumed and suppressed throughout this paper.

II. Paraxial Surface Field Formulation

Consider an elementary surface electric current source given by

$$\mathbf{J}_e = \left(P_e^z \hat{z} + P_e^\phi \hat{\phi}\right) \frac{\delta(\phi - \phi')\delta(z - z')}{d} \tag{1}$$

located on the surface of a dielectric coated circular cylinder whose geometry is given in Fig. 1 ($\rho = \rho' = d$). The surface

Manuscript received July 16, 2000; revised August 23, 2001.

V. B. Ertürk is with the Department of Electrical and Electronics Engineering, Bilkent University, TR-06533, Bilkent, Ankara, Turkey.

R. G. Rojas is with the The Ohio State University, Department of Electrical Engineering, ElectroScience Laboratory, Columbus, OH 43212-1191 USA.

Digital Object Identifier 10.1109/TAP.2002.803955

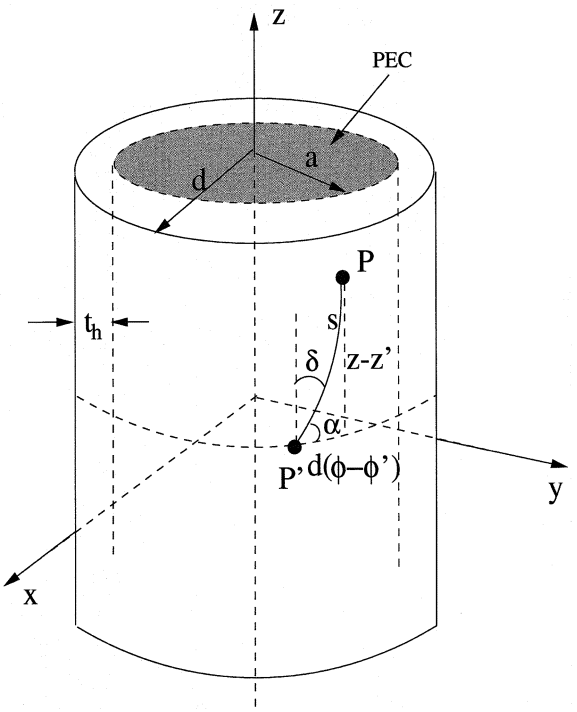

Fig. 1. Dielectric coated PEC circular cylinder where the radius of the PEC cylinder is a and the thickness of the dielectric coating is $t_h = d - a$.

field component in the l-direction ($l = \phi$ or z) at $\rho = d$ excited by a u-directed source defined in (1) ($u = \phi$ or z) can be written as

$$E_l(z,\phi) = \frac{1}{2\pi}\sum_{n=-\infty}^{\infty} e^{jn(\phi-\phi')} \times \int_{-\infty}^{\infty} \frac{G_{lu}(n,k_z)}{2\pi d} P_e^u e^{-jk_z(z-z')} dk_z \quad (2)$$

where $G_{lu}(n,k_z)$ is the ρ-propagating series representation of the appropriate dyadic Green's function component which is explicitly given in [9] for both source and observation points located on the surface ($\rho = \rho' = d$). In this paper, we are only interested in the tangential components of the surface fields due to the tangential current sources since most of the moment method based conformal printed antenna analysis/design algorithms require the use of these components. Therefore, the ρ-components, which might be important for applications involving an excitation via a probe, are not considered here due to space limitations. However, note that the computation of the normal components are similar to that of the tangential components considered here.

It is known that the series in (2) converges very slowly for electrically large cylinders because the Green's function involves Bessel and Hankel functions along with their derivatives. Their computation for large values of n is not a trivial matter due to the numerical instabilities that occur when the order and argument of these functions become large. Therefore, (2) can be transformed into a more rapidly convergent ϕ-propagating series representation by using the Watson's transformation [9]. Provided that the cylinder is electrically large (at least one wavelength in radius), it is enough to retain the leading term.

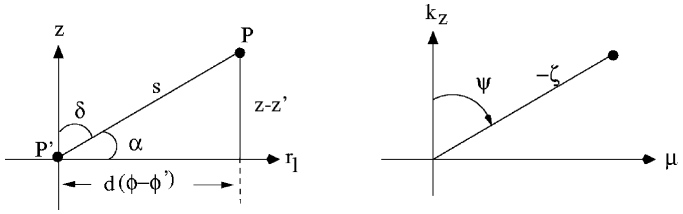

Fig. 2. Space (s,δ) and spectral (ζ,ψ) polar coordinates (after [15]).

As a result of this process, the surface field component is given by

$$E_l(z,\phi) \approx \frac{1}{2\pi}\int_{-\infty}^{\infty}\int_{-\infty-j\epsilon}^{\infty-j\epsilon} \frac{G_{lu}(\nu,k_z)}{2\pi d} P_e^u \times e^{-jk_z(z-z')} e^{-j\nu(\phi-\phi')} d\nu dk_z, \qquad \epsilon > 0. \quad (3)$$

The integral given by (3) can be expressed in polar coordinates by performing the following transformations [15]

$$k_z = -\zeta\cos\psi, \quad \nu = \mu d \text{ where } \mu = -\zeta\sin\psi \quad (4)$$

and

$$r_l = d(\phi-\phi') = s\sin\delta, \quad (z-z') = s\cos\delta \quad (5)$$

where the definitions of ψ, δ, s, and ζ are shown in Fig. 2. The result of this procedure can be written as

$$E_l(s,\delta) \approx \frac{1}{2\pi}\int_0^{\infty}\int_0^{2\pi} \frac{G_{lu}(\zeta,\psi)}{2\pi} P_e^u e^{j\zeta s\cos(\psi-\delta)} d\psi\zeta d\zeta. \quad (6)$$

The inner integral of (6) can be evaluated asymptotically in closed form with respect to ψ using the stationary phase method [16] where the stationary points [the point(s) where the most significant contribution to the integral occurs] are at $\psi_s = \delta$ and $\psi_s = \delta+\pi$. Applying this method to (6) and keeping the leading term, yields

$$E_l(s,\delta) \approx \frac{1}{2\pi}\int_0^{\infty} P_e^u \left[\frac{G_{lu}(\zeta,\delta)}{2\pi}\sqrt{\frac{2\pi}{s\zeta}} e^{j(s\zeta-(\pi/4))} + \frac{G_{lu}(\zeta,\delta+\pi)}{2\pi}\sqrt{\frac{2\pi}{s\zeta}} e^{j(-s\zeta+(\pi/4))}\right]\zeta d\zeta. \quad (7)$$

An analysis with respect to ψ reveals that the tangential components of the dyadic Green's function are periodic with π (i.e., $G_{lu}(\zeta,\psi) = G_{lu}(\zeta,\psi+\pi)$) and hence, (7) becomes

$$E_l(s,\delta) \approx \frac{1}{2\pi}\int_0^{\infty} G_{lu}(\zeta,\delta) P_e^u \sqrt{\frac{2}{s\pi\zeta}}\cos\left(s\zeta-\frac{\pi}{4}\right)\zeta d\zeta. \quad (8)$$

Noting that $\sqrt{2/s\pi\zeta}\cos(s\zeta-\pi/4)$ is the large argument approximation for the Bessel function $J_o(s\zeta)$ [18], (8) can be approximately written as

$$E_l(s,\delta) \approx \frac{1}{2\pi}\int_0^{\infty} J_0(s\zeta) G_{lu}(\zeta,\delta) P_e^u \zeta d\zeta. \quad (9)$$

Note that expression (9) is similar to the leading term of the surface field expression for the planar case (infinite radius of curvature) [17]. Although expressions (8) and (9) do not yield accurate results within the paraxial region for some field components, they serve as a guide for the development of a more

accurate paraxial formulation. The accuracy of (8) and (9) can be improved by adding the second term in the stationary phase integration, however, an alternative approach is followed here.

Keeping in mind that $G_{lu}(\zeta,\psi)$ is periodic in ψ (with period of $T=\pi$), it can be represented by a FS, namely

$$G_{lu}(\zeta,\psi)\approx\sum_{n=0}^{N}a_n(\zeta)\cos n2\psi+\sum_{n=1}^{N}b_n(\zeta)\sin n2\psi \quad (10)$$

where $a_n(\zeta)$ and $b_n(\zeta)$ are coefficients given by

$$a_n(\zeta)=\frac{\epsilon_n}{\pi}\int_T G_{lu}(\zeta,\psi)\cos n2\psi d\psi \quad (11)$$

$$b_n(\zeta)=\frac{2}{\pi}\int_T G_{lu}(\zeta,\psi)\sin n2\psi d\psi \quad (12)$$

where $\epsilon_n=1$, for $n=0$ and $\epsilon_n=2$, for $n\neq 0$. As seen in (11) and (12), the FS coefficients are only functions of ζ. As a result of this, the variables ζ and ψ are separated in the approximate Green's function representation simplifying the surface field calculations significantly. The FS coefficients are calculated using numerical integration, namely

$$a_n(\zeta)\approx\frac{\epsilon_n}{\pi}\sum_{p=1}^{P}w_pG_{lu}(\zeta,\psi_p)\cos n2\psi_p \quad (13)$$

$$b_n(\zeta)\approx\frac{2}{\pi}\sum_{p=1}^{P}w_pG_{lu}(\zeta,\psi_p)\sin n2\psi_p \quad (14)$$

where w_p are the appropriate weights. The stationary phase method shows that the strongest contributions to the ψ-integral come from $\psi=\delta$ and $\psi=\pi+\delta$ ($\delta=0$ along the axial direction). Thus, to obtain a valid solution within the paraxial region, the Green's function components $G_{lu}(\zeta,\psi)$ should be exact at least at $\psi=0$ and $\psi=\pi$. Using this information, the abscissas in (13) and (14) should include these two points. An additional benefit is that the expressions for $G_{lu}(\zeta,\psi)$ become much simpler when $\psi_p=0,\pi/2$ and π (due to the terms involving $\sin\psi$, $\cos\psi$), resulting in a simpler numerical integration with respect to ζ in (6).

Although the essence of the method is the same for all components, each of them has certain unique features and hence, has been treated slightly different as discussed in Sections II-A–C.

A. $G_{zz}(\zeta,\psi)$ Component

In addition to its periodicity, $G_{zz}(\zeta,\psi)$ is even with respect to ψ yielding $b_n=0$. Furthermore, based on numerical experimentation, including the leading two terms gives enough accuracy for this component. Therefore, using a three-point trapezoidal rule [18] in the interval $[0,\pi]$ for the calculation of $a_{0_{zz}}$ and $a_{1_{zz}}$, yields the following simple expressions:

$$a_{0_{zz}}(\zeta)\approx\frac{1}{2}\left[G_{zz}(\zeta,\psi=0)+G_{zz}\left(\zeta,\psi=\frac{\pi}{2}\right)\right] \quad (15)$$

$$a_{1_{zz}}(\zeta)\approx\frac{1}{2}\left[G_{zz}(\zeta,\psi=0)-G_{zz}\left(\zeta,\psi=\frac{\pi}{2}\right)\right] \quad (16)$$

where the identity $G_{zz}(\zeta,\psi=\pi)=G_{zz}(\zeta,\psi=0)$ has been used to simplify the expressions. Substituting (15) and (16) into (10), $G_{zz}(\zeta,\psi)$ is given by

$$G_{zz}(\zeta,\psi)\approx G_{zz}\left(\zeta,\psi=\frac{\pi}{2}\right)+\left[G_{zz}(\zeta,\psi=0)-G_{zz}\left(\zeta,\psi=\frac{\pi}{2}\right)\right]\left(\frac{1+\cos 2\psi}{2}\right). \quad (17)$$

A similar approximate form is given in [15] (although it was obtained in a heuristic fashion). The expression in (17) is exact at $\psi=0$ (and also at $\psi=\pi$). This implies that using (17) in (6) yields accurate results around the paraxial region ($\delta\to 0$ or $\alpha\to\pi/2$). However, it loses accuracy as δ becomes large for large values of s.

B. $G_{\phi z}(\zeta,\psi)=G_{z\phi}(\zeta,\psi)$ Component

The $G_{\phi z}(\zeta,\psi)$ component, which is an odd function with respect to ψ, is written as

$$G_{\phi z}(\zeta,\psi)=\frac{\zeta^2\sin 2\psi}{2}\tilde{G}_{\phi z}(\zeta,\psi) \quad (18)$$

where $\tilde{G}_{\phi z}(\zeta,\psi)$ is $G_{\phi z}(\zeta,\psi)$ as defined in [9], except that $(\nu/d)k_z=\mu k_z=(\zeta^2\sin 2\psi)/2$ is excluded. $\tilde{G}_{\phi z}(\zeta,\psi)$, which is an even function in ψ, is approximated with a FS where including only the leading term gives enough accuracy. The FS coefficients for $\tilde{G}_{\phi z}(\zeta,\psi)$ can be obtained in the same fashion as the FS coefficients of $G_{zz}(\zeta,\psi)$. Thus, the FS coefficient $a_{0_{\phi z}}$ is calculated performing a numerical integration in the $[0,\pi]$ interval using a two-point trapezoidal rule and is given by

$$a_{0_{\phi z}}\approx\frac{1}{\pi}\left[\frac{\pi}{2}\left(\tilde{G}_{\phi z}(\zeta,\psi=0)+\tilde{G}_{\phi z}(\zeta,\psi=\pi)\right)\right]=\tilde{G}_{\phi z}(\zeta,\psi=0) \quad (19)$$

yielding

$$G_{\phi z}(\zeta,\psi)\approx\frac{\zeta^2\sin 2\psi}{2}\tilde{G}_{\phi z}(\zeta,\psi=0) \quad (20)$$

which is exact at $\psi=0$. Numerical results reveal that if we use (20) in (6), accurate results are obtained around the paraxial region $\delta\to 0$ ($\alpha\to\pi/2$), but the accuracy deteriorates as δ increases for large separations (large s).

C. $G_{\phi\phi}(\zeta,\psi)$ Component

Evaluation of this component differs from the others because the methods used for the calculation of the components $G_{zz}(\zeta,\psi)$ and $G_{z\phi}(\zeta,\psi)$ do not yield results with enough accuracy. Therefore, $G_{\phi\phi}(\zeta,\psi)$ is written as the sum of *planar* + *curvature correction* terms, namely

$$G_{\phi\phi}(\zeta,\psi)\approx G^{p}_{uu}(\zeta,\psi)+G^{cc}_{\phi\phi}(\zeta,\psi) \quad (21)$$

where $u=x$ or y and p denotes "planar" whereas cc stands for "curvature correction." The planar term, $G^{p}_{uu}(\zeta,\psi)$, corresponds to a cylinder with an infinitely large radius of curvature. It is written as

$$G^{p}_{uu}(\zeta,\psi)=G^{p1}_{uu}(\zeta)-G^{p2}_{uu}(\zeta)\left(\frac{1-\cos 2\psi}{2}\right)\zeta^2. \quad (22)$$

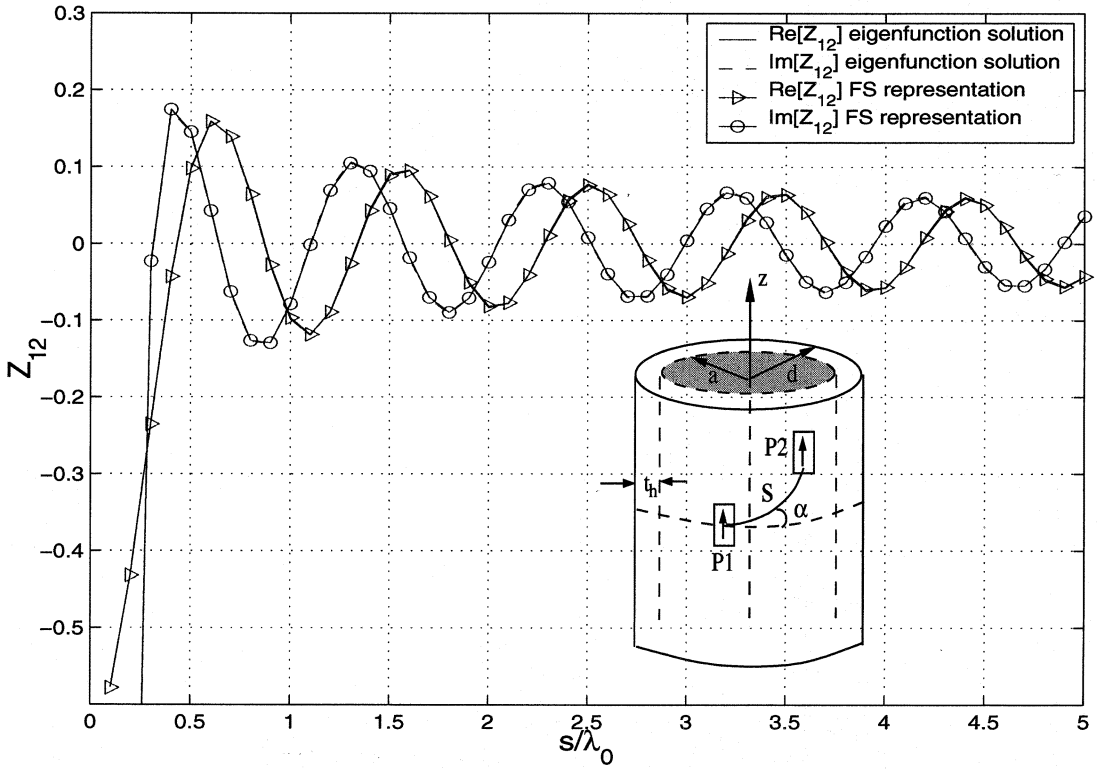

Fig. 3. Real and imaginary parts of the mutual impedance (Z_{12}) between two identical z-directed current sources ($\alpha = 90°$) for a coated cylinder with $a = 3\lambda_0$, $t_h = 0.06\lambda_0$, $\epsilon_r = 3.25$.

Note that, the planar term $G^p_{uu}(\zeta,\psi)$ is already written as a two term FS expansion in ψ and can be integrated in closed-form with respect to ψ. However, the curvature correction term, $G^{cc}_{\phi\phi}(\zeta,\psi)$, has a behavior similar to $G_{zz}(\zeta,\psi)$. It is an even function in ψ which implies that $b_n = 0$. Furthermore, based on numerical experimentation, including the first two terms of the FS expansion gives accurate results. After an extensive testing of different numerical integration routines and number of sample points, accurate numerical results are obtained for $a_{0_{\phi\phi}}$ and $a_{1_{\phi\phi}}$ with the following algorithm:

$$a_{0_{\phi\phi}} \approx \frac{1}{4}\left[G^{cc}_{\phi\phi}(\zeta,\psi=0) + G^{cc}_{\phi\phi}\left(\zeta,\psi=\frac{\pi}{2}\right)\right] \tag{23}$$

$$a_{1_{\phi\phi}} \approx \frac{1}{4}\left[G^{cc}_{\phi\phi}(\zeta,\psi=0) - G^{cc}_{\phi\phi}\left(\zeta,\psi=\frac{\pi}{2}\right)\right]. \tag{24}$$

As a result of this process, the final expression for the curvature correction term becomes

$$G^{cc}_{\phi\phi}(\zeta,\psi) \approx \frac{1}{2}\Bigg\{G^{cc}_{\phi\phi}(\zeta,\psi=0) + \left[G^{cc}_{\phi\phi}\left(\zeta,\psi=\frac{\pi}{2}\right) - G^{cc}_{\phi\phi}(\zeta,\psi=0)\right] \times \left(\frac{1-\cos 2\psi}{2}\right)\Bigg\}. \tag{25}$$

Combining (22) with (25), the Green's function component $G_{\phi\phi}(\zeta,\psi)$ is given by

$$G_{\phi\phi}(\zeta,\psi) \approx G^{p1}_{uu}(\zeta) + \frac{1}{2}G^{cc}_{\phi\phi}(\zeta,\psi=0) + \Bigg\{-\zeta^2 G^{p2}_{uu}(\zeta) + \frac{1}{2}\left[G^{cc}_{\phi\phi}\left(\zeta,\psi=\frac{\pi}{2}\right) - G^{cc}_{\phi\phi}(\zeta,\psi=0)\right] \times \left(\frac{1-\cos 2\psi}{2}\right)\Bigg\}. \tag{26}$$

As in the $G_{zz}(\zeta,\psi)$ and $G_{z\phi}(\zeta,\psi)$ cases, using (26) in (6) yields accurate results around the paraxial region ($\delta \to 0$ or $\alpha \to \pi/2$), however it loses accuracy as δ becomes large for large values of s.

Equations (17), (20), and (26) are the components of the approximate space domain Green's function representation which are substituted into (6) to find the surface fields due to tangential current elements located on the coating. In all components, the common feature is the separation of the ζ and ψ variables which allows the closed-form integration with respect to ψ in (6). Substituting (17), (20), and (26) into (6), and calculating the ψ integrals in closed form, the following expressions are obtained for the surface fields:

$$E_{zz}(\delta,s) \approx \frac{-Z_0 p^z_e}{2\pi k_0} \times \left\{k_0^2 P(s) + \frac{\partial^2}{\partial z^2}\left[P(s) - Q(s)\right]\right\} \tag{27}$$

$$E_{\phi z}(\delta,s) \approx \frac{-Z_0 p^z_e}{2\pi k_0}\frac{\partial^2}{\partial z \partial r_l}\left\{M(s) - R(s)\right\} \tag{28}$$

$$E_{\phi\phi}(\delta,s) \approx \frac{-Z_0 p^\phi_e}{2\pi k_0}\left\{k_0^2 U(s) + \frac{\partial^2}{\partial r_l^2} \times \left[U(s) - \frac{\epsilon_r - 1}{\epsilon_r}W(s)\right]\right\}$$

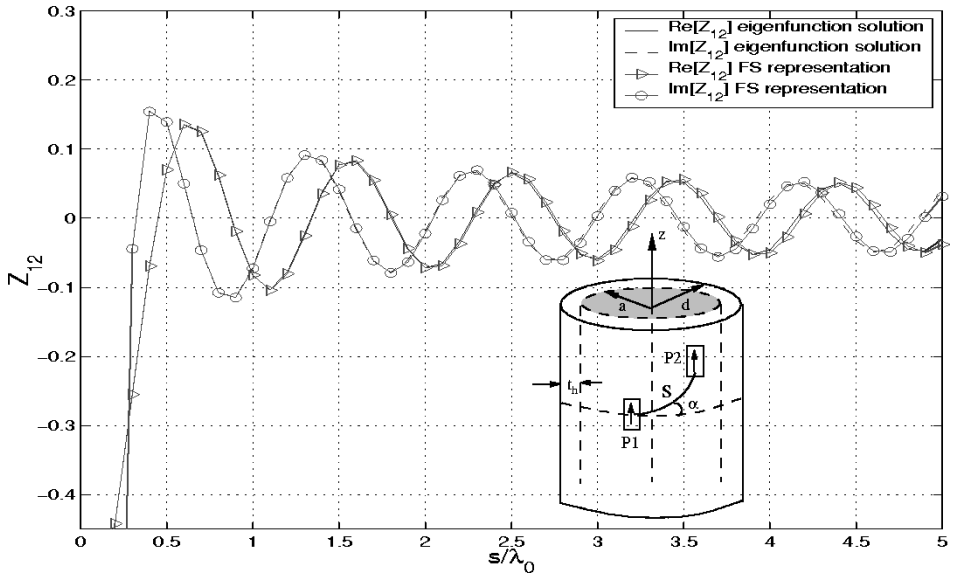

Fig. 4. Real and imaginary parts of the mutual impedance (Z_{12}) between two identical z-directed current sources $(\alpha = 70^\circ)$ for a coated cylinder with $a = 3\lambda_0$, $t_h = 0.06\lambda_0$, $\epsilon_r = 3.25$.

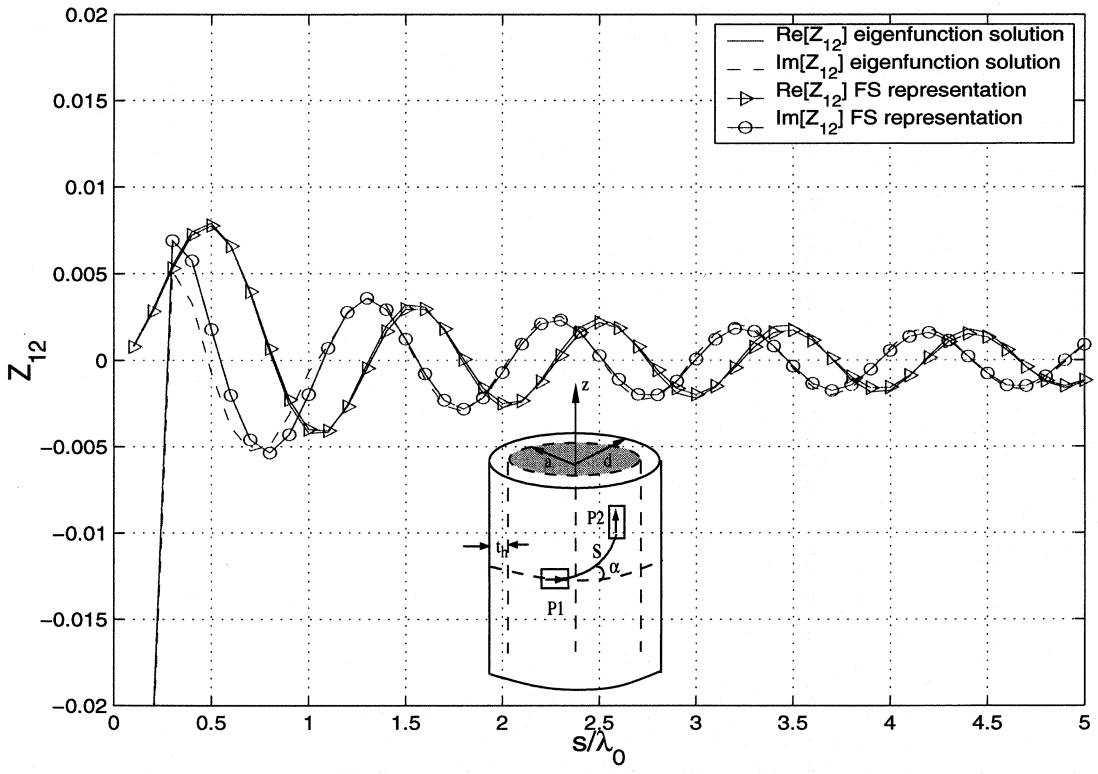

Fig. 5. Real and imaginary parts of the mutual impedance (Z_{12}) between z- and ϕ-directed current sources $(\alpha = 88^\circ)$ for a coated cylinder with $a = 3\lambda_0$, $t_h = 0.06\lambda_0$, $\epsilon_r = 3.25$.

$$+\frac{jZ_0 p_e^{\phi}}{2\pi k_0}\left\{S(s)+\frac{\partial^2}{\partial r_l^2}T(s)\right\} \tag{29}$$

where $P(s)$, $Q(s)$, $M(s)$, $R(s)$, $W(s)$, $U(s)$, $S(s)$, and $T(s)$ are given in (31) through (75), respectively, in Appendix 1. Note, that $U(s)$ and $W(s)$ are exactly the same special functions defined in [17] (special functions used for the Sommerfeld integral representation for the single layer microstrip dyadic Green's function) for the planar case.

The ζ-integrals are evaluated numerically along the real axis using a Gaussian quadrature algorithm. In all functions, except $R(s)$, $S(s)$, and $T(s)$, an envelope extraction technique is used to overcome the difficulties in the numerical integration arising from their oscillatory as well as slowly decaying behavior of the integrands. The special functions $R(s)$, $S(s)$, and $T(s)$ are relatively smooth and absolutely integrable. Therefore, the use of an envelope extraction technique to integrate these functions is not required. Furthermore, the singularities which are on the

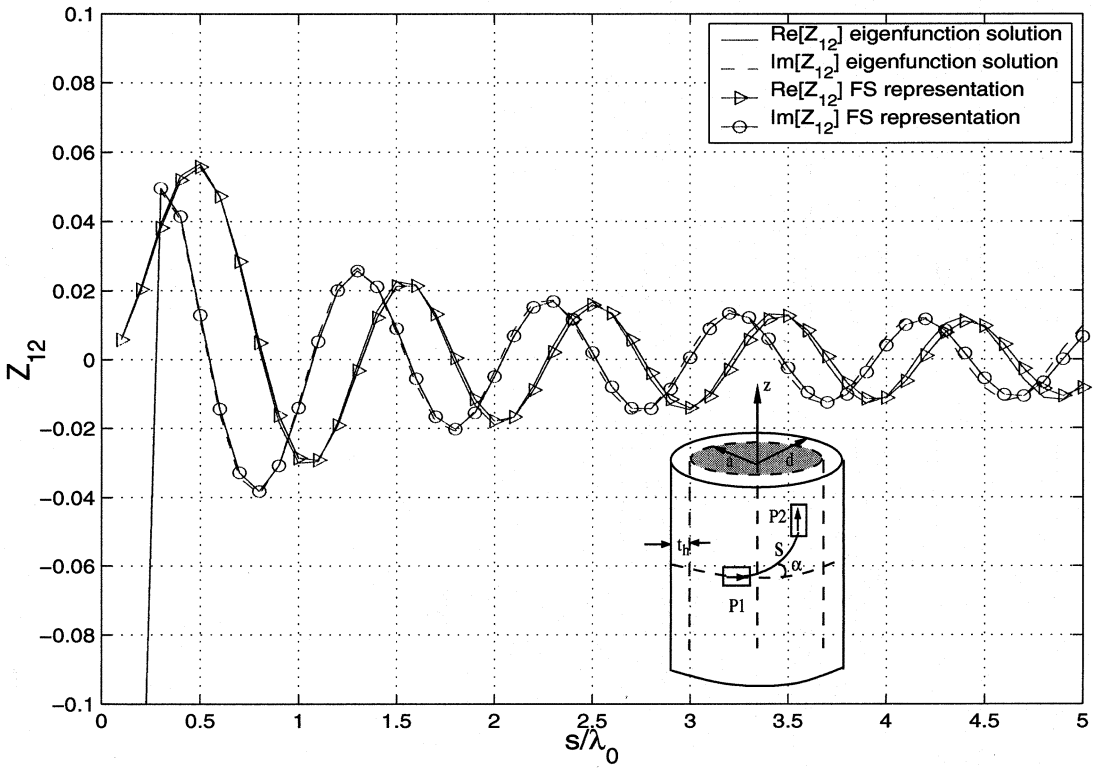

Fig. 6. Real and imaginary parts of the mutual impedance (Z_{12}) between z- and ϕ-directed current sources ($\alpha = 75°$) for a coated cylinder with $a = 3\lambda_0$, $t_h = 0.06\lambda_0$, $\epsilon_r = 3.25$.

real axis (for lossless case) along the path of integration are handled by regularizing the integrands. To implement this step, the singularities are found by means of a Newton–Raphson method.

III. Numerical Results

To assess the accuracy of this method, numerical results for the mutual impedance between two tangential electric current modes are obtained using (27)–(29) and compared with a standard eigenfunction solution given by (2) for a large cylinder with $a = 3\lambda_0$, $t_h = 0.06\lambda_0$, $\epsilon_r = 3.25$ (λ_0 = free-space wavelength). Note that the mutual impedance Z_{nm} between the current modes is simply given by

$$Z_{nm} = \int_{S_m} \mathbf{E}_n \cdot \mathbf{J}_m ds \tag{30}$$

where $\mathbf{E}_n$ is the field due to source (current mode) $\mathbf{J}_n$ and S_m is the area occupied by source (current mode) $\mathbf{J}_m$. The current modes are defined by a piecewise sinusoid along the direction of the current and by a constant along the direction perpendicular to the current. Each element has dimensions of $0.05\lambda_0$ (along the direction of the current) by $0.02\lambda_0$. This particular choice of current modes guarantees the convergence of the reference spectral domain solution (2) for large cylinders, even though the rate of convergence is very slow. In all figures, the real and imaginary parts of the mutual impedance between two current modes are plotted versus separation. For each component, the results are given for various values of the angle (α).

Figs. 3 and 4 depict the mutual impedance between two z-directed sources for α equals to 90° and 70°, respectively. As expected, the mutual coupling is strongest for $\alpha = 90°$ (in the same direction of the current sources) and becomes weaker as α moves away from the axial direction. The oscillatory nature of the coupling as the separation changes indicates that there are at least two types of field contributions adding in and out of phase. Note that for the planar case [19] the sum of space and surface wave contributions also results in a curve that oscillates.

The next set of results, namely, Figs. 5 and 6, show the mutual impedance between a z- and a ϕ-directed current sources. Keeping in mind that the mutual impedance is zero along the axial direction, the angle α has been set to 88° and 75°. In this case, the mutual impedance becomes stronger as α moves away from the axial direction. Actually, it can be shown [20] that it reaches at maximum at some angle around 45° and starts to decrease again as α approaches 0°. The oscillations also become stronger as α approaches 45°.

Figs. 7 and 8 show the last set of numerical results for the mutual impedance between two ϕ-directed current sources for $\alpha = 90°$ and $\alpha = 70°$, respectively. Note that the mutual impedance is slightly stronger when $\alpha = 90°$ compared to $\alpha = 70°$. As a matter of fact, it can be shown [20] that the mutual coupling for this case is maximum at $\alpha = 0°$, reaches a minimum at some angle α larger or equal to 45° (it depends on the value of s/λ_0) and begins to increase again as α approaches 90° (the axial direction).

In all numerical results shown here, the agreement between the reference solution and the new paraxial expressions is excel-

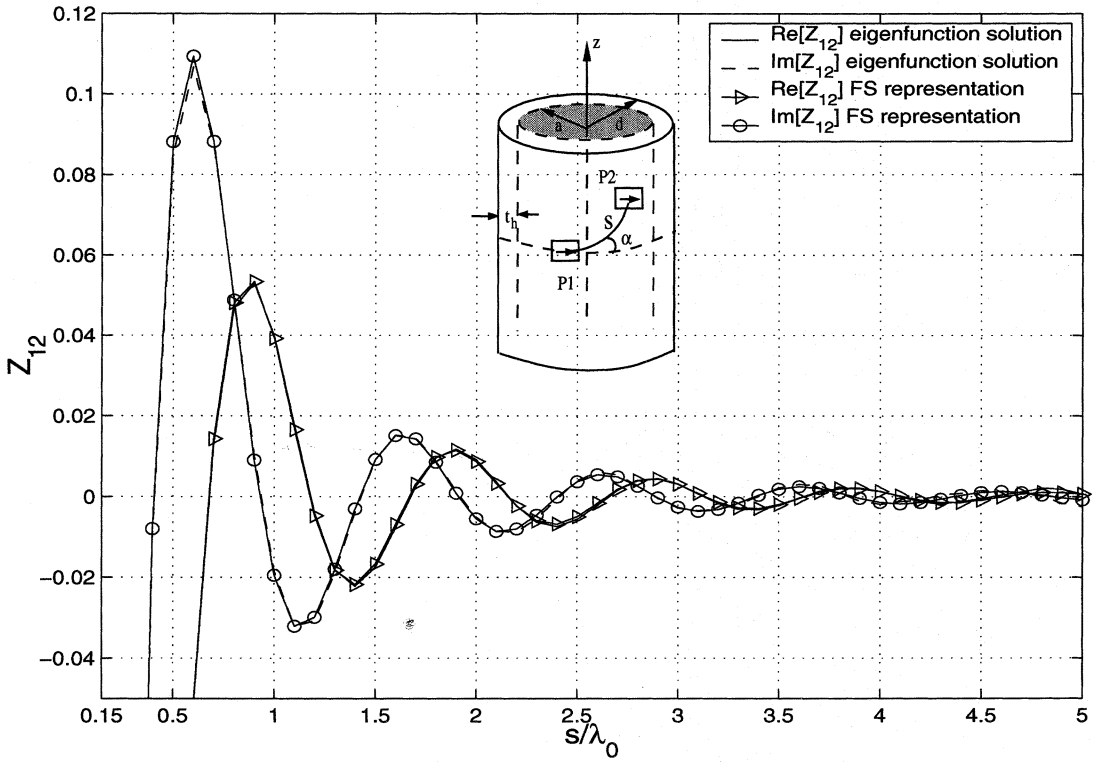

Fig. 7. Real and imaginary parts of the mutual impedance (Z_{12}) between two identical ϕ-directed current sources ($\alpha = 90°$) for a coated cylinder with $a = 3\lambda_0$, $t_h = 0.06\lambda_0$, $\epsilon_r = 3.25$.

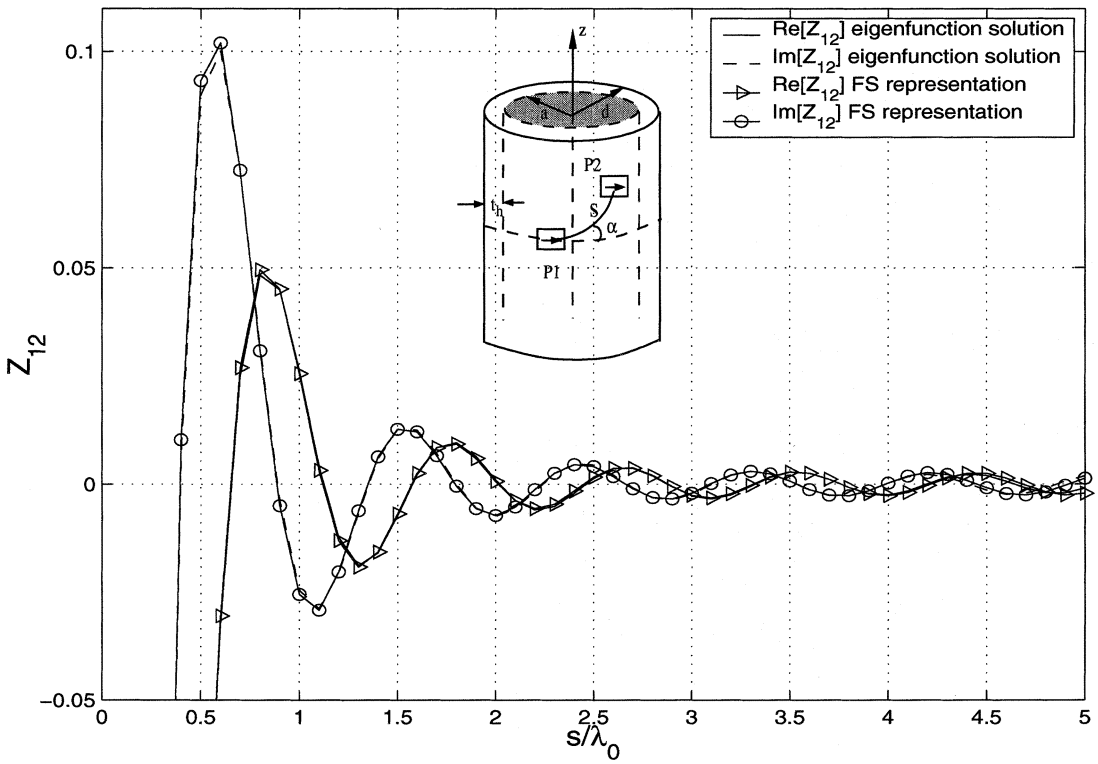

Fig. 8. Real and imaginary parts of the mutual impedance (Z_{12}) between two identical ϕ-directed current sources ($\alpha = 70°$) for a coated cylinder with $a = 3\lambda_0$, $t_h = 0.06\lambda_0$, $\epsilon_r = 3.25$.

lent. On the other hand, the CPU time for the proposed method is approximately five times faster than the reference solution for this particular cylinder. Moreover, the elapsed CPU time for the solution presented here is fairly independent from the size of the cylinder's radius (for radii $\geq \lambda_o$), whereas, the elapsed CPU time for the eigenfunction solution increases as the electrical size of the cylinder's radius becomes larger. This clearly shows that the present method is a much more efficient for large cylinders than the standard eigenfunction solution.

IV. Discussion and Conclusion

An efficient and accurate scheme for the evaluation of surface fields within the paraxial region of an electrically large dielectric coated circular cylinder is developed. These surface fields are excited by electric current sources mounted on the surface of the coated cylinder. Note that most previously published results for large cylinders (with or without coating) fail to yield accurate results in the paraxial region.

The essence of this representation is based on the fact that the circumferentially propagating series representation of the appropriate Green's function is periodic and hence,can be approximated by a Fourier series. Based on numerical experimentation, it appears that only the two leading terms of the expansion yield enough accuracy in most cases. The accuracy of this Green's function as well as the ease of its evaluation are determined by the type of integration algorithm used to calculate the Fourier series coefficients. The algorithm used here is based on information obtained from the stationary phase points of the ψ integral in (6).

This novel representation of the Green's function for a large coated cylinder, which complements previously published asymptotic representations [9], can be used in conjunction with the method of moments to analyze and design arbitrarily shaped conformal printed antennas on coated cylinders. Finally, for some of the field components, the scheme developed here can be made valid for regions outside the paraxial region (arbitrary values of the angle α) with some minor modifications.

Appendix

The special functions used in (27)–(29) are given by

$$P(s) = \int_0^\infty \frac{\zeta}{jT_m^{\pi/2}(\zeta)} J_0(\zeta s) d\zeta \tag{31}$$

$$Q(s) = \int_0^\infty \frac{k_0^2 - \zeta^2}{j\zeta} \left\{ \frac{1}{T_m^0(\zeta)} - \frac{1}{T_m^{\pi/2}(\zeta)} \right\} \times J_0(\zeta s)\, d\zeta \tag{32}$$

$$M(s) = \int_0^\infty \frac{\zeta}{jT_m^0(\zeta)} J_0(\zeta s)\, d\zeta \tag{33}$$

$$R(s) = \int_0^\infty \frac{k_0^2(\epsilon_r - 1)}{k_1^2 - \zeta^2} \frac{\zeta\sqrt{k_0^2 - \zeta^2} R^0(\zeta)}{jT_m^0(\zeta) T_e^0(\zeta)} J_0(\zeta s) d\zeta \tag{34}$$

$$W(s) = \int_0^\infty \frac{\zeta\sqrt{k_0^2 - \zeta^2}}{Dp_1 Dp_2} J_0(\zeta s) d\zeta \tag{35}$$

$$U(s) = \int_0^\infty \frac{\zeta}{Dp_1} J_0(\zeta s) d\zeta \tag{36}$$

where

$$Dp_1(\zeta) = \sqrt{k_0^2 - \zeta^2} - j\sqrt{k_1^2 - \zeta^2} \times \cot\left[t_h \sqrt{k_1^2 - \zeta^2} \right] \tag{37}$$

$$Dp_2(\zeta) = \sqrt{k_0^2 - \zeta^2} + \frac{j\sqrt{k_1^2 - \zeta^2}}{\epsilon_r} \times \tan\left[t_h \sqrt{k_1^2 - \zeta^2} \right] \tag{38}$$

$$T_{\substack{m \\ e}}^0(\zeta) = \sqrt{k_0^2 - \zeta^2} R^0(\zeta) - \frac{k_0^2 - \zeta^2}{k_1^2 - \zeta^2} C_{\substack{m \\ e}}^0(\zeta) \tag{39}$$

$$T_{\substack{m \\ e}}^{\pi/2}(\zeta) = k_0 R^{\pi/2}(\zeta) - C_{\substack{m \\ e}}^{\pi/2}(\zeta) \tag{40}$$

with

$$R^0(\zeta) = -j - \frac{1}{2d\sqrt{k_0^2 - \zeta^2}} \tag{41}$$

$$R^{\pi/2}(\zeta) = \begin{cases} \frac{H_{(\zeta d)}^{(2)'}(k_0 d)}{H_{(\zeta d)}^{(2)}(k_0 d)} & \left| \frac{\zeta}{k_0} - 1 \right| \leq \frac{1}{d^{2/3}} \\ -j\frac{\sqrt{k_0^2 - \zeta^2}}{k_0} - \frac{1}{2d} \frac{k_0}{\left(k_0^2 - \zeta^2\right)}, & \text{elsewhere} \end{cases} \tag{42}$$

$$C_m^0 = \epsilon_r \left[\frac{\sqrt{k_1^2 - \zeta^2}}{\tan\left[t_h \sqrt{k_1^2 - \zeta^2} \right]} - \frac{1}{2d} \right] \tag{43}$$

$$C_e^0 = \frac{-\sqrt{k_1^2 - \zeta^2}}{\cot\left[t_h \sqrt{k_1^2 - \zeta^2} \right]} + \frac{1}{2d} \tan^2\left[t_h \sqrt{k_1^2 - \zeta^2} \right] \tag{44}$$

$$C_m^{\pi/2} = \frac{\sqrt{k_1^2 - \zeta^2}}{\tan\left[t_h \sqrt{k_1^2 - \zeta^2} \right]} - \frac{1}{2d} \left\{ \frac{k_1^2}{k_1^2 - \zeta^2} - \frac{t_h^2 \zeta^2}{\sin^2\left[t_h \sqrt{k_1^2 - \zeta^2} \right]} \right\} \tag{45}$$

$$C_e^{\pi/2} = \frac{-\sqrt{k_1^2 - \zeta^2}}{\epsilon_r \cot\left[t_h \sqrt{k_1^2 - \zeta^2} \right]} + \frac{1}{2d\epsilon_r} \left\{ \frac{t_h^2 \zeta^2}{\cos^2\left[t_h \sqrt{k_1^2 - \zeta^2} \right]} + \frac{k_1^2 \tan^2\left[t_h \sqrt{k_1^2 - \zeta^2} \right]}{k_1^2 - \zeta^2} \right\}. \tag{46}$$

$$A_0\begin{pmatrix}0\\ \pi/2\end{pmatrix}(\zeta) = -j\sqrt{k_0^2-\zeta^2}\,S_1\begin{pmatrix}0\\ \pi/2\end{pmatrix}(\zeta) \tag{52}$$

$$A_1\begin{pmatrix}0\\ \pi/2\end{pmatrix}(\zeta) = 0.5\left[j\sqrt{k_0^2-\zeta^2}\,S_2\begin{pmatrix}0\\ \pi/2\end{pmatrix}(\zeta) - \left(-2dC_{fx}\begin{pmatrix}0\\ \pi/2\end{pmatrix}(\zeta)\right) S_1\begin{pmatrix}0\\ \pi/2\end{pmatrix}(\zeta)\right] \tag{53}$$

$$A_2\begin{pmatrix}0\\ \pi/2\end{pmatrix}(\zeta) = 0.25\left[j\sqrt{k_0^2-\zeta^2}\,S_3\begin{pmatrix}0\\ \pi/2\end{pmatrix}(\zeta) + \left(-2dC_{fx}\begin{pmatrix}0\\ \pi/2\end{pmatrix}(\zeta)\right) S_2\begin{pmatrix}0\\ \pi/2\end{pmatrix}(\zeta)\right] \tag{54}$$

$$A_3\begin{pmatrix}0\\ \pi/2\end{pmatrix}(\zeta) = 0.125\left(-2dC_{fx}\begin{pmatrix}0\\ \pi/2\end{pmatrix}(\zeta)\right) S_3\begin{pmatrix}0\\ \pi/2\end{pmatrix}(\zeta) \tag{55}$$

$$T_0\begin{pmatrix}0\\ \pi/2\end{pmatrix}(\zeta) = Pl_1\begin{pmatrix}0\\ \pi/2\end{pmatrix}(\zeta)\,Pl_2\begin{pmatrix}0\\ \pi/2\end{pmatrix}(\zeta) \tag{56}$$

$$T_1\begin{pmatrix}0\\ \pi/2\end{pmatrix}(\zeta) = -0.5\left[Pl_1\begin{pmatrix}0\\ \pi/2\end{pmatrix}(\zeta)\tilde{C}_2\begin{pmatrix}0\\ \pi/2\end{pmatrix}(\zeta) + Pl_2\begin{pmatrix}0\\ \pi/2\end{pmatrix}(\zeta)\tilde{C}_1\begin{pmatrix}0\\ \pi/2\end{pmatrix}(\zeta)\right] \tag{57}$$

$$T_2\begin{pmatrix}0\\ \pi/2\end{pmatrix}(\zeta) = 0.25\tilde{C}_1\begin{pmatrix}0\\ \pi/2\end{pmatrix}(\zeta)\tilde{C}_2\begin{pmatrix}0\\ \pi/2\end{pmatrix}(\zeta) \tag{58}$$

$$S_1\begin{pmatrix}0\\ \pi/2\end{pmatrix}(\zeta) = N_1\begin{pmatrix}0\\ \pi/2\end{pmatrix}(\zeta)\,Pl_1\begin{pmatrix}0\\ \pi/2\end{pmatrix}(\zeta) \tag{59}$$

$$S_2\begin{pmatrix}0\\ \pi/2\end{pmatrix}(\zeta) = N_1\begin{pmatrix}0\\ \pi/2\end{pmatrix}(\zeta)\tilde{C}_1\begin{pmatrix}0\\ \pi/2\end{pmatrix}(\zeta) - N_2\begin{pmatrix}0\\ \pi/2\end{pmatrix}(\zeta)\,Pl_1\begin{pmatrix}0\\ \pi/2\end{pmatrix}(\zeta) \tag{60}$$

$$S_3\begin{pmatrix}0\\ \pi/2\end{pmatrix}(\zeta) = N_2\begin{pmatrix}0\\ \pi/2\end{pmatrix}(\zeta)\tilde{C}_1\begin{pmatrix}0\\ \pi/2\end{pmatrix}(\zeta) \tag{61}$$

$$N_1^0(\zeta) = \frac{k_0^2}{k_1^2-\zeta^2}\left(\frac{-\sqrt{k_1^2-\zeta^2}}{\cot\left[t_h\sqrt{k_1^2-\zeta^2}\right]}\right) \tag{62}$$

$$N_2^0(\zeta) = \frac{k_0^2}{k_1^2-\zeta^2}\tan^2\left[t_h\sqrt{k_1^2-\zeta^2}\right] \tag{63}$$

$$N_1^{\pi/2}(\zeta) = \frac{1}{\epsilon_r}\left(\frac{-\sqrt{k_1^2-\zeta^2}}{\cot\left[t_h\sqrt{k_1^2-\zeta^2}\right]}\right) \tag{64}$$

$$N_2^{\pi/2}(\zeta) = \frac{1}{\epsilon_r}\left[\frac{t_h^2\zeta^2}{\cos^2\left[t_h\sqrt{k_1^2-\zeta^2}\right]} + \frac{k_1^2}{k_1^2-\zeta^2}\tan^2\left[t_h\sqrt{k_1^2-\zeta^2}\right]\right] \tag{65}$$

$$Pl_1^0(\zeta) = -j\sqrt{k_0^2-\zeta^2} - \epsilon_r\left(\frac{k_0^2-\zeta^2}{k_1^2-\zeta^2}\right)\frac{\sqrt{k_1^2-\zeta^2}}{\tan\left[t_h\sqrt{k_1^2-\zeta^2}\right]} \tag{66}$$

$$Pl_2^0(\zeta) = -j\sqrt{k_0^2-\zeta^2} + \left(\frac{k_0^2-\zeta^2}{k_1^2-\zeta^2}\right)\frac{\sqrt{k_1^2-\zeta^2}}{\cot\left[t_h\sqrt{k_1^2-\zeta^2}\right]} \tag{67}$$

$$Pl_1^{\pi/2}(\zeta) = -j\sqrt{k_0^2-\zeta^2} - \frac{\sqrt{k_1^2-\zeta^2}}{\tan\left[t_h\sqrt{k_1^2-\zeta^2}\right]} \tag{68}$$

$$S^{\binom{0}{\pi/2}}(s)=\int_0^\infty \frac{\mathrm{Num}_1^{\binom{0}{\pi/2}}(\zeta)d^2+\mathrm{Num}_2^{\binom{0}{\pi/2}}(\zeta)d+A_3^{\binom{0}{\pi/2}}(\zeta)}{T_0^{\binom{0}{\pi/2}}(\zeta)\left[T_0^{\binom{0}{\pi/2}}(\zeta)d^2+T_1^{\binom{0}{\pi/2}}(\zeta)d+T_2^{\binom{0}{\pi/2}}(\zeta)\right]}\frac{J_0(\zeta s)}{\zeta d}d\zeta \tag{49}$$

$$Pl_2^{\pi/2}(\zeta)=-j\sqrt{k_0^2-\zeta^2}+\frac{1}{\epsilon_r}\left(\frac{\sqrt{k_1^2-\zeta^2}}{\cot\left[t_h\sqrt{k_1^2-\zeta^2}\right]}\right) \tag{69}$$

$$\tilde{C}_1^0(\zeta)=1-\epsilon_r\frac{k_0^2-\zeta^2}{k_1^2-\zeta^2} \tag{70}$$

$$\tilde{C}_2^0(\zeta)=1+\left(\frac{k_0^2-\zeta^2}{k_1^2-\zeta^2}\right)\tan^2\left[t_h\sqrt{k_1^2-\zeta^2}\right] \tag{71}$$

$$\tilde{C}_1^{\pi/2}(\zeta)=-2dC_{fx}^{\pi/2}(\zeta)-\left(\frac{k_1^2}{k_1^2-\zeta^2}-\frac{t_h^2\zeta^2}{\sin^2\left[t_h\sqrt{k_1^2-\zeta^2}\right]}\right) \tag{72}$$

$$\tilde{C}_2^{\pi/2}(\zeta)=-2dC_{fx}^{\pi/2}(\zeta)+\frac{1}{\epsilon_r}\left(\frac{t_h^2\zeta^2}{\cos^2\left[t_h\sqrt{k_1^2-\zeta^2}\right]}+\frac{k_1^2}{k_1^2-\zeta^2}\tan^2\left[t_h\sqrt{k_1^2-\zeta^2}\right]\right) \tag{73}$$

The special functions $S(s)$ and $T(s)$, which are related to the curvature correction term, are given by

$$S(s)=\zeta^2S^0(s) \tag{47}$$

and

$$T(s)=S^{\pi/2}(s)-S^0(s) \tag{48}$$

where [please refer to (49) at the top of this page] and

$$\mathrm{Num}_1^{\binom{0}{\pi/2}}(\zeta)=A_1^{\binom{0}{\pi/2}}(\zeta)T_0^{\binom{0}{\pi/2}}(\zeta)-A_0^{\binom{0}{\pi/2}}(\zeta)T_1^{\binom{0}{\pi/2}}(\zeta) \tag{50}$$

$$\mathrm{Num}_2^{\binom{0}{\pi/2}}(\zeta)=A_2^{\binom{0}{\pi/2}}(\zeta)T_0^{\binom{0}{\pi/2}}(\zeta)-A_0^{\binom{0}{\pi/2}}(\zeta)T_2^{\binom{0}{\pi/2}}(\zeta). \tag{51}$$

The functions used in (49)–(51) are defined in (52)–(68) on the previous page and (69)–(73) at the top of this page, and finally

$$C_{fx}^{\pi/2}(\zeta)=\begin{cases}j\sqrt{k_0^2-\zeta^2}+k_0\frac{H_{(\zeta d)}^{(2)\prime}(k_0d)}{H_{(\zeta d)}^{(2)}(k_0d)}, & \left|\frac{\zeta}{k_0}-1\right|\le\frac{1}{d^{2/3}}\\ -\frac{1}{2d}\frac{k_0^2}{(k_0^2-\zeta^2)}, & \text{elsewhere.}\end{cases} \tag{74}$$

$$C_{fx}^0(\zeta)=-\frac{1}{2d}. \tag{75}$$

Note, that a superscript 0' or $\pi/2$' denotes that a function is evaluated at $\psi=0$ or $\psi=\pi/2$, respectively. In all these expressions k_0 is the free-space wavenumber and $k_1=\sqrt{\epsilon_r}k_0$ is the wavenumber inside the dielectric medium with a relative permittivity $\epsilon_r>1$.

REFERENCES

[1] A. Nakatini, N. G. Alexopoulus, N. K. Uzunoglu, and P. L. E. Uslenghi, "Accurate Green's function computation for printed circuit antennas on cylindrical antennas," *Electromagn.*, vol. 6, pp. 243–254, July–Sept. 1986.

[2] T. M. Habashy, S. M. Ali, and J. A. Kong, "Input impedance and radiation pattern of cylindrical-rectangular and wraparound microstrip antennas," *IEEE Trans. Antennas Propagat.*, vol. 38, pp. 722–731, May 1990.

[3] K. Naishadham and L. B. Felsen, "Dispersion of waves guided along a cylindrical substrate-superstrate layered medium," *IEEE Trans. Antennas Propagat.*, vol. 41, pp. 304–313, Mar. 1993.

[4] L. W. Pearson, "A construction of the fields radiated by a z-directed point sources of current in the presence of a cylindrically layered obstacle," *Radio Sci.*, vol. 21, pp. 559–569, July–Aug. 1986.

[5] K.-L. Wong, *Design of Nonplanar Microstrip Antennas and Transmission Lines*. New York: Wiley, 1999.

[6] P. Munk, "A Uniform Geometrical Theory of Diffraction for the Radiation and Mutual Coupling Associated With Antennas on a Material Coated Convex Conducting Surface," Ph.D. dissertation, The Ohio State Univ., Dept. Elect. Eng., 1996.

[7] C. Demirdag and R. G. Rojas, "Mutual coupling calculations on a dielectric coated PEC cylinder using UTD-based green's function," in *Proc. IEEE Antennas Propagat. Symp. Dig.*, vol. 3, Montreal, Canada, July 1997, pp. 1525–1528.

[8] R. G. Rojas and V. B. Ertürk, "UTD ray analysis of mutual coupling and radiation for antennas mounted on dielectric coated PEC convex surfaces," in *Proc. URSI Int. Symp. Electromagn. Theory*, vol. 1, May 1998, pp. 178–180.

[9] V. B. Ertürk and R. G. Rojas, "Efficient computation of surface fields excited on a dielectric coated circular cylinder," *IEEE Trans. Antennas Propagat.*, vol. 48, pp. 1507–1516, Oct. 2000.

[10] Z. W. Chang, L. B. Felsen, and A. Hessel, "Surface Ray Methods for Mutual Coupling in Conformal Arrays on Cylinder and Conical Surfaces," Polytech. Inst., New York, 1976.
[11] S. W. Lee and S. Safavi-Naini, "Asymptotic Solution of Surface Field Due to a Magnetic Dipole on a Cylinder," Univ. Illinois at Urbana–Champaign, Dept. Elect. Eng., 76-11, 1976.
[12] P. H. Pathak and N. Wang, "An Analysis of the Mutual Coupling Between Antennas on a Smooth Convex Surface," The Ohio State Univ. ElectroSci. Lab. Dept. Elect. Eng., 784 538-7, 1978.
[13] J. Boersma and S. W. Lee, "Surface Field Due to a Magnetic Dipole on a Cylinder: Asymptotic Expansion of Exact Solution," Univ. Illinois at Urbana–Champaign, Dept. Elect. Eng., 78-17, 1978.
[14] R. J. Pogorzelski, "On the high-frequency asymptotic evaluation of the potentials of elemental sources on an anisotropic impedance cylinder," *Radio Sci.*, vol. 31, pp. 389–399, Mar.–Apr. 1996.
[15] M. Marin and P. Pathak, "Calculation of Surface Fields Created by a Current Distribution on a Coated Circular Cylinder," The Ohio State Univ. ElectroSci. Lab. Dept. Elect. Eng., 721 565-1, 1989.
[16] L. B. Felsen and N. Marcuvitz, *Radiation and Scattering of Waves*. Englewood Cliffs, NJ: Prentice-Hall, 1973.
[17] S. Barkeshli, "Efficient Approaches for Evaluating the Planer Microstrip Green's Function and Its Applications to the Analysis of Microstrip Antennas," Ph.D. dissertation, The Ohio State Univ. Dept. Elect. Eng., 1987.
[18] M. Abramowitz and I. A. Stegun, *Handbook of Mathematical Functions*. New York: Dover, 1970.
[19] S. Barkeshli, P. H. Pathak, and M. Marin, "An asymptotic closed-form microstrip closed-form microstrip Green's function for the efficient moment method analysis of mutual coupling in microstrip antennas," *IEEE Trans. Antennas Propagat*, vol. 38, pp. 1374–1383, Sept. 1990.
[20] V. B. Ertürk, "Efficient Hybrid MoM/Green's Function Technique to Analyze Conformal Microstrip Antennas and Arrays," Ph.D. dissertation, The Ohio State Univ., Dept. Elect. Eng., 2000.

V. B. Ertürk received the B.S. degree in electrical engineering from the Middle East Technical University, Ankara, Turkey, and the M.S. and Ph.D. degrees from The Ohio State University, (OSU), Columbus, in 1993, 1996, and 2000, respectively.

Currently, he is an Assistant Professor with the Department of Electrical and Electronics Engineering, Bilkent University, Ankara, Turkey. His research interests include design and analysis of active and passive microstrip antennas and arrays on planar and curved surfaces.

R. G. Rojas received the B.S.E.E. degree from New Mexico State University, University Park, NM, and the M.S. and Ph.D, degrees in electrical engineering form The Ohio State University (OSU), Columbus, in 1979, 1981, and 1985, respectively.

Currently, he is a Professor with the Department of Electrical Engineering, OSU. His research interests include the analysis and design of conformal arrays, active integrated arrays, nonlinear microwave circuits, as well as the analysis of electromagnetic radiation and scattering phenomena in complex environments.

Dr. Rojas was the recipient of the 1988 R.W.P. King Prize Paper Award, the 1990 Browder J. Thompson Memorial Prize Award, both awarded by IEEE, and the Lumley Research Awards, given by the College of Engineering, OSU, in 1989 and 1993. He has served as Chairman, Vice Chairman, and Secretary/Treasurer of the IEEE Antennas and Propagation, and Microwave Theory and Technique Societies, Columbus, OH Chapter. He is a Member of the U.S. Commission B of URSI.